Aerodynamic and Flight Dynamic Analysis of Finned Re-Entry Vehicles

JOHN K. KRYVORUKA* AND WILLIAM T. ASHURST†
Sandia Laboratories, Livermore, Calif.

A computational method is presented for predicting nonlinear aerodynamic characteristics of finned re-entry configurations and (by computer simulation) the effect of these characteristics on vehicle flight stability. These aerodynamic characteristics, which include induced roll and yaw effects, are highly dependent on inviscid surface cross-flow. This cross-flow is often severe enough to produce large induced roll moments which can negate the control effect of the fins and in some cases generate severe flight instabilities. The important cross-flow effects on fins are accurately determined by an approximation to the circumferential momentum equation. Particular attention is given to a representation of the fin roll and yaw characteristics with analytic functions of angle of attack and fin cant. Computer simulations indicate that the adverse cross-flow effects for a variable cant, two-fin roll-control system can be dramatically reduced by the addition of two fixed-cant fins. The validity of the analytic methods for fin aerodynamic characteristics and the trajectory simulation technique is fully established by means of a flight test in which the unique four-fin control system maintained vehicle roll and yaw stability through a severe roll resonance encounter. Actual roll rate and flight-derived fin aerodynamic characteristics are in excellent agreement with predictions, thus verifying the analysis.

Nomenclature

δ_c	= geometric fin cant
δ_f	= surface cross-flow angle
r, u θ, v ϕ, w	= coordinates, velocities in spherical coordinate system, origin of cone apex
ρ	= fluid density
ϕ	= vehicle roll orientation relative to angle of attack plane
η	= cone bluntness ratio (nose radius/base radius)
C_{N_f}	= fin normal force coefficient
C_l	= total fin rolling moment coefficient
$C_l(\delta_c, \alpha)$	= fin rolling moment coefficient due to fin cant
$C_{l_{\delta_c}}$	= fin cant coefficient derivative $\delta C_l(\delta_c, \alpha)/\partial\delta_c$
$C_{l\phi_1}, C_{l\phi_2}$	= induced rolling moment coefficients due to roll orientation
α	= vehicle total angle of attack
C_N	= induced vehicle yawing moment coefficient in body axes
C_m, C_n	= induced vehicle pitch and yaw moment coefficients in rolling axes
$P(\phi)$	= cone surface pressure
p_{crit}	= vehicle natural pitch frequency
M_∞	= freestream Mach number
θ_c	= vehicle cone angle
A_{fin}	= fin planform area
A_{base}	= vehicle base reference area
D_{base}	= vehicle base diameter—reference length
$\bar{\chi}$	= distance from fins to mass center in calibers

Introduction

BALLISTIC re-entry vehicles (RV's) are plagued by anomalous roll rate behavior—including spin-up, roll reversal,[1] and persistent roll resonance[2]—which can lead to large impact dispersions or even catastrophic flight failure. These roll anomalies arise from small aerodynamic and mass asymmetries.[3] Since these asymmetries are often ablation-induced, even an initially perfect RV may still have flight instabilities. Therefore, it seems probable that roll-control mechanisms could improve RV flight performance: Several roll-control concepts—such as fins,[4,5] flaps, and reaction jets[6]—have been proposed and developed. This paper considers one particular type of roll-control: variable-cant, external, aerodynamic spin fins. Historically, the fins on sounding rockets have produced severe flight dynamic instabilities with respect to roll and angular motion (Nicolaides[7]). More recently, Platus[5] has shown similar dynamic instabilities by considering a sharp cone with a pair of fixed-cant fins with the fin aerodynamics treated in Newtonian fashion. The cross-flow effect becomes a sinusoidal function of the roll angle with amplitude equal to the angle of attack added to the fin cant. The motivation for the present analysis was the desire to generate a more general computational method that would be appropriate for large angles of attack and for blunt cones. While the capability exists for a full three-dimensional flowfield solution, a more efficient scheme is desirable for extensive system analysis of possible roll-control mechanisms.

The purpose of the study described in this paper was twofold: first, to obtain a detailed understanding of the nonlinear aerodynamics of hypersonic finned RV's and the associated effects on flight performance; and second, to use the resulting aerodynamic characteristics to select a fin roll-control configuration that does not introduce roll or yaw dynamic instabilities. A computational technique which properly accounts for cross-flow is presented and verified by experiment.[4]

Spin Fin Aerodynamics

In this analysis, the fin height is assumed to be much greater than the boundary-layer thickness, much less than the shock-layer thickness, and the inviscid body surface flow is used to estimate the fin force. For nonzero angles of attack, the higher windward pressure produces a cross-flow that alters the direction of the inviscid surface flow and changes the effective fin attack angle, and, hence, the roll torque. The cross-flow is symmetric about the angle-of-attack plane and is zero at the windward and leeward rays. Fin roll torque depends upon surface pressure and effective attack angle, α_{fin}, which is comprised of the fin cant angle, δ_c, plus the cross-flow angle, δ_f (Fig. 1).

Presented as Paper 73-183 at the AIAA 11th Aerospace Sciences Meeting, Washington, D.C., January 10–12, 1973; submitted July 27, 1973; revision received November 19, 1973. This work was supported by the U.S. Atomic Energy Commission.

Index categories: Entry Vehicle Dynamics and Control; Supersonic and Hypersonic Flow.

* Member of Technical Staff, Exploratory Systems Dept. Member AIAA.

† Member of Technical Staff, Exploratory Systems Dept.

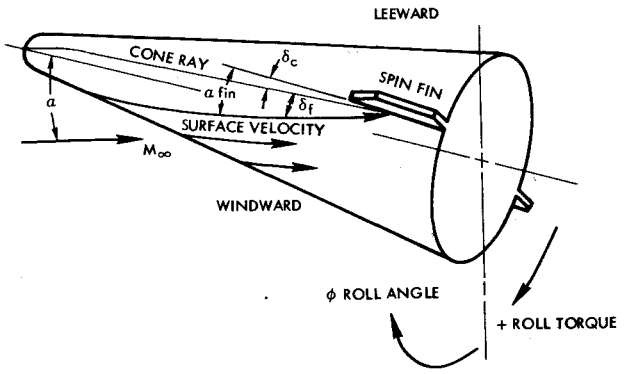

Fig. 1 Spin fin aerodynamics.

Chrusciel and Hull[8] have shown that it is feasible to use the tangent cone concept, combined with bluntness effects, to realistically describe nonlinear aerodynamic behavior of sphere cones. The universal expressions for sphere cone pressures developed by Blick and Francis[9] have been incorporated into a computer program (FANDY) for sphere-cone aerodynamic estimates.[11] A simple estimate has been developed for cone surface cross-flow which allows FANDY to provide realistic estimates of the nonlinear aerodynamics of spin fins. (Program FANDY was created by adding this cross-flow solution to the previously developed program HANDY.[11])

Cross-Flow Determination

For an inviscid estimate, consider the cross-flow momentum which is being driven primarily by the circumferential pressure gradient $\partial P/\partial\phi$. The steady-state flow continuity and circumferential ϕ momentum equations for a spherical coordinate system with the origin at the cone apex are combined to yield an approximate equation for the cross-flow velocity at the cone surface

$$w\,\partial w/\partial\phi + wu\sin\theta_c + (1/\rho)\,\partial p/\partial\phi \approx 0$$

The r derivatives have been dropped, and the cross-flow velocity variation in the θ direction has also been assumed to be negligible. The cross-flow velocity is zero at the windward and leeward planes with nonzero circumferential derivatives. In the program HANDY,[11] pressures at $\phi = 0°$, 90°, and 180° are determined from tangent-cone theory and Blick's sphere-cone pressure distributions and provide the coefficients for a three-term cosine polynomial. Hence, $\partial P/\partial\phi$ is known. Replacing $\partial w/\partial\phi$ by $(w_\phi - w_{\phi-\Delta\phi})\Delta\phi$ yields a quadratic equation for w. Nodal spacings of 5° and 10° in $\Delta\phi$ provide smooth results for w vs ϕ at small angles of attack. Due to the approximate equations being used, the value of w at the leeward plane was not zero for large angles of attack. Therefore, for roll angles greater than 120°, a straight line decay to zero at 180° was used.

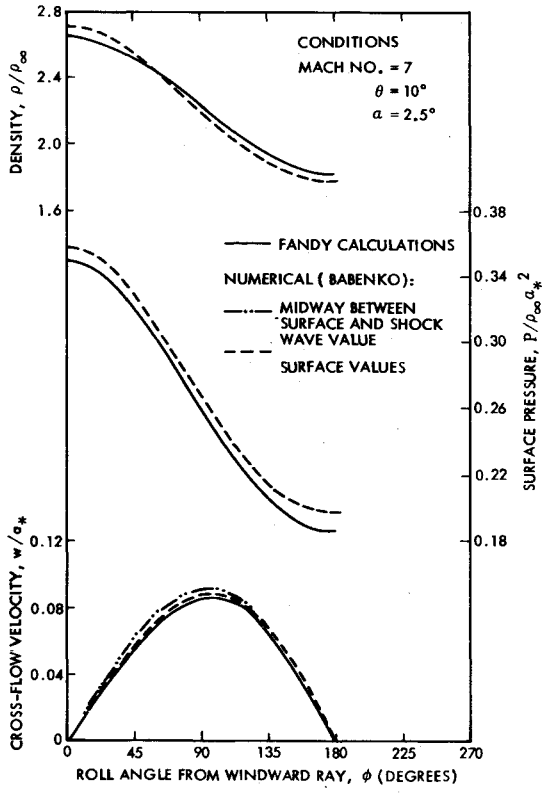

Fig. 2 Comparison of FANDY calculations of surface density, pressure, and cross-flow velocity vs roll angle for a sharp cone with Babenko's numerical solution.

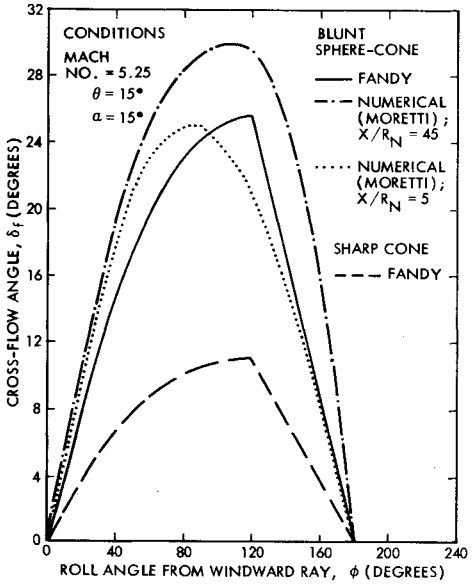

Fig. 3 Comparison of FANDY calculations of cross-flow angle for sharp and blunt sphere-cones with Moretti's numerical solution for a blunt sphere-cone.

The FANDY estimates agree very well with the exact numerical solutions of Babenko et al.[12] Figure 2 presents a comparison of the circumferential variation of density, pressure, and cross-flow velocity for a sharp, 10° cone in Mach 7 flow at a 2.5° angle of attack. The exact cross-flow velocity halfway between the body and the shock wave is shown by a dashed line in Fig. 2. It appears that the assumption of small variation of the cross-flow velocity in the θ direction is valid for sharp cones. Good agreement with the exact results is also found at an angle of attack of 5° (Ref. 13).

Due to the blunt cone's normal shock, its surface density is much less than that of a sharp cone. However, the pressure distribution approaches sharp cone values for $X\theta_c^2/R_n \geqq 1$ (see Ref. 9). Thus, the cross-flow velocity increases as the surface density decreases in order to maintain the same cross-flow momentum. Since the surface axial velocity is not greatly changed for blunt and sharp cones, the cross-flow angles are much larger for blunt cones.

FANDY estimates are given in Fig. 3 for the cross-flow angle, δ_f ($\delta_f = \tan^{-1} w/u$) of a blunt and a sharp 15° cone at a 15° attack angle. The blunt-cone solution using Moretti's computer program[10] is also shown. For a 15° sphere cone, sharp-cone pressure values should be approached for $X/R_n \gtrsim 15$. Thus, the Moretti results indicate about a 10% axial variation in δ_f caused by bluntness effects. The FANDY calculation for

large X/R_n is in reasonable agreement with the blunt sphere cone solution using Moretti's program. The FANDY calculation also shows that the cross-flow angle for a sharp cone has about half the magnitude of the cross-flow angle for a blunt cone.

It was mentioned earlier that the cross-flow angle for a sharp cone is almost constant between the body and the shock wave. Rakich and Cleary[14] calculated that the cross-flow angle for a blunt cone approaches the sharp-cone value at about 20%–40% of the distance from the body to the shock (see Fig. 9 in Ref. 14). The effect of neglecting the cross-flow gradient in the θ direction is not known because the Moretti results between the body and the shock wave were not smooth enough to allow gradient determination. However, as will be shown later, the surface value seems to be estimated adequately for force correlation for fins of short exposed span.

Rakich and Cleary also point out that the viscous cross-flow angle is much larger than the inviscid cross-flow angle. Consequently, cross-flow angles as determined from an oil-film experiment (e.g., George[15]) would yield values too large for the inviscid cross-flow. Results from FANDY for the maximum cross-flow angle as a function of total angle of attack are shown in Fig. 4. Experiments for a 10° sphere cone at an angle of attack of less than 5° show the maximum cross-flow angle is approximately equal to the angle of attack for a typical sharp cone ($\eta \leqq 0.05$) and is four times the angle of attack for a typical blunt cone ($\eta = 0.25$). Consequently, there may be roll orientations and RV angles of attack which make the cross-flow angle greater than a given fin cant angle. Thus, the fin roll torque magnitude and direction will depend on the roll and attack of angles. If the torque associated with a pair of fins reverses as the body angle of attack is increased, the behavior of the roll-control system could become unstable. The Newtonian analysis by Platus produces a maximum cross-flow angle equal to the angle of attack. This analysis is certainly valid for sharp cones at small angles of attack (smaller than the cone angle). However, the application of sharp cone fin aerodynamics to blunt cones is incorrect.

Fin Force Calculation

The FANDY program is used to perform fin force calculations. For each desired roll angle ϕ, the fin cant is added to the local cross-flow angle δ_f to provide the total fin angle of attack α_{fin}. The fin aerodynamic environment is specified by α_{fin}, local cone surface Mach number M_s, and pressure $P(\phi)$. The fin force is calculated by using an attached, oblique shock for the fin's windward pressure and a Prandtl-Meyer expansion for the fin's leeward pressure. For these calculations, the fin is assumed to be a thin, flat plate with exposed span so short that the specified fin area is immersed in a uniform flow appropriate to the local flow conditions at the RV surface. Oblique shocks corresponding to either a planar wedge or a conical shock may be used for calculating the windward pressure on the fin. The axisymmetric flow of the latter produces a lower pressure than the wedge shock and may approximate pressure losses due to span effects. Comparison with unpublished wind tunnel data for fin-pair roll torque indicates that the conical shock assumption provides fin estimates with, at most, $\pm 20\%$ disagreement.

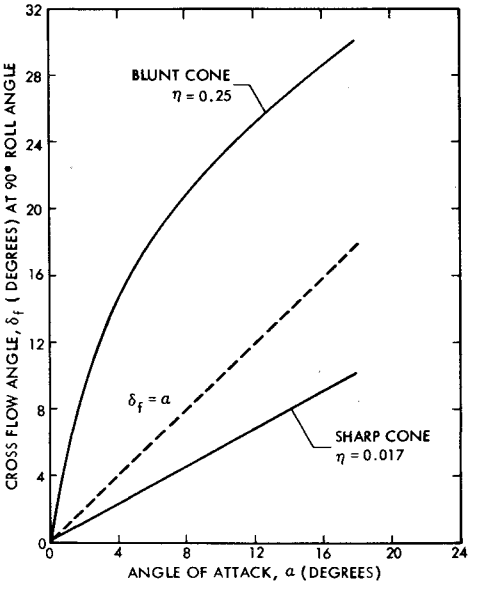

Fig. 4 Maximum cone surface cross-flow angle (at 90° roll angle) for sharp and blunt 10° cones.

Fin Force Expression

For trajectory simulation, it is desirable to specify the fin aerodynamic environment, and hence the fin force, with a set of parameters that are convenient for a model roll-control system to determine. Rather than cone surface Mach number and pressure, a geometric set of parameters has been selected. Therefore, for a given freestream Mach number, the fin force is expressed as a function of 1) fin cant angle, δ_c, 2) roll angle, ϕ, and 3) body angle of attack, α. The fin forces calculated by FANDY have been expressed as powers of δ_c and α and as a Fourier expansion in roll orientation angle. For the range of 360°, the force on one fin may adequately be described as follows:

$$C_{N_f} = A_0 + A_1 \cos\phi + A_2 \cos 2\phi + B_1 \sin\phi + B_2 \sin 2\phi \quad (1)$$

where the A's and B's are functions of δ_c and α and are determined from the calculational procedure.

Roll Moment Coefficient

Torque and forces for a pair of fins diametrically opposed are easily found by combining the torque caused by one fin at ϕ and cant δ_c, with the second fin torque at $\phi_2 = \phi_1 + 180°$ and cant δ_2.

For a pair of fins with equal fin cant angle, the period is reduced to 180° because the fins are indistinguishable and a rotation of 180° produces the initial fin positions. The fin-pair roll coefficient with equal fin cant is expressed as

$$C_l = C_{l_{\delta_c}}(\alpha)\delta_c + C_{l\phi_1}(\alpha, \delta_c)\sin 2\phi + C_{l\phi_2}(\alpha, \delta_c)\cos 2\phi \quad (2)$$

The first term in Eq. (2) represents the roll moment coefficient due to fin cant only (no cross-flow effect). This term is approximately linear in the fin cant δ_c, and has been expressed as $C_{l_{\delta_c}}(\alpha)\delta_c$. The next two terms represent the cross-flow effect, and their amplitudes are nonlinear functions of the angle of attack and vanish for angle of attack equal to zero. From symmetry requirements with respect to angle of attack and roll angle, the following functional forms were deduced

$$C_{l\delta_c}(\alpha) = a_0 + a_2\alpha^2 + a_4\alpha^4 \quad (3)$$

$$C_{l\delta_1}(\alpha, \delta_c) = b_2\alpha^2 + b_4\alpha^4 \quad (4)$$

$$C_{l\phi_2}(\alpha, \delta_c) = c_2\alpha^2 + c_4\alpha^4 \quad (5)$$

The constants b and c have small variations with respect to fin cant angle δ_c (powers zero, two, and four). Thus, while the cross-flow induced terms are nearly independent of fin cant, the roll independent term is linearly coupled to geometric fin cant. This important distinction is utilized later.

To demonstrate the subtleties of these nonlinear fin-pair roll torque coefficients, calculations are presented for a sharp and a blunt cone. The example used is a 10° sphere cone with bluntness ratios (η) of 0.017 and 0.25 at Mach 10 and a pair of coupled spin fins (equal cant) located at the cone base station. Each fin planform area is 0.01 of the cone base area with the fin lever arm equal to the base radius. The calculated roll coefficients are presented in Fig. 5 for the sharp cone and in Fig. 6 for the blunt cone.

Several important observations can be made. First, the amplitude of the $\cos 2\phi$ term is an order of magnitude smaller than the $\sin 2\phi$ term. The induced nonlinearity arising from the cross-flow, is therefore, essentially embodied in $C_{l\phi_1}$. Second,

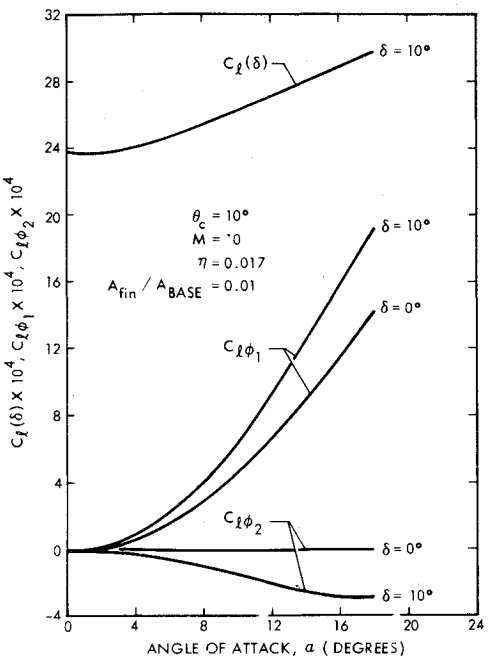

Fig. 5 Fin pair rolling moment coefficients for sharp cone.

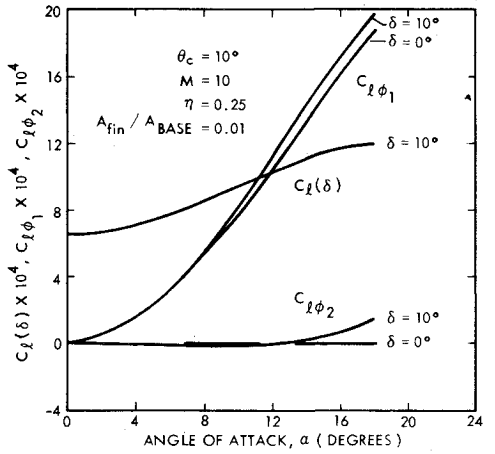

Fig. 6 Fin pair rolling moment coefficients for blunt cone.

the induced roll moment coefficients are strong functions of angle of attack but are nearly independent of fin cant, particularly for the blunt configuration. That is, large cross-flow nonlinearities exist even for the case of zero geometric fin cant. Third, all coefficients increase with increasing angle of attack. However, at high angles of attack, the fin cant coefficient begins to decrease, and indications are that for large enough fin cant and vehicle angle of attack the fin will stall. Fourth, the induced roll moment coefficient can become large enough to contribute substantially to the total roll moment coefficient. Depending on roll orientation, this effect will either assist or severely degrade the roll control capability of the fins for both the sharp and blunt cones. From Fig. 6 it can be seen that for the blunt cone at angles of attack greater than about 12°, the induced roll moment exceeds the fin cant moment. Therefore, at certain roll orientations, the fins lose their roll control effectiveness.

Yaw Force and Moment

The yaw force and moment arising from the differential fin effectiveness are obtained from Eq. (1) by assuming equal fin cants ($\delta_1 = \delta_2 = \delta$) with one fin at roll orientation ϕ and the second at $\phi_2 = \phi + 180°$. The yaw moment in the rolling body axes may be expressed (neglecting differential fin drag) as

$$C_n = (-2A_1 \sin\phi - 2B_1 \cos\phi)\bar{\chi} \tag{6}$$

Calculated values are presented in Fig. 7 for both sharp and blunt cones at a 12° angle of attack. In nonrolling axes, the induced pitch and yaw moments caused by the fins are

$$C_M = 2\bar{\chi}(A_1 \sin^2\phi + B_1 \sin\phi \cos\phi) \tag{7}$$

$$C_N = -2\bar{\chi}(A_1 \sin\phi \cos\phi + B_1 \cos^2\phi) \tag{8}$$

Equations (7) and (8) can be compared directly with the results obtained by Platus.[5] His linearized analysis produces relationships among the coefficients of Eq. (1) that these calculations show are too small. The induced yaw moment will produce, in certain cases, a dynamic instability resulting in a divergence of the vehicle angle of attack.

Flight Dynamics

Nicolaides[7] has shown that severe instabilities (roll lock-in and catastrophic yaw) occur on high fineness ratio configurations such as sounding rockets as a result of induced fin nonlinearities. Platus[5] has demonstrated the existence of dynamic instabilities on re-entry configurations for the case of two diametrically opposed fixed-cant fins. The latter analysis indicates the presence of a Magnus-type yaw instability due to differential fin effectiveness. In the present analysis, the effects of induced roll nonlinearities on flight performance are demonstrated by incorporating the theoretical fin aerodynamics (developed in the previous section for the blunt cone) into a trajectory simulation in which the complete equations of motion[16] are solved.

The blunt cone configuration discussed previously is used in the trajectory simulation. The vehicle also has an aerodynamic asymmetry which produces a 1° nonrolling trim angle and an out-of-plane center-of-mass offset $y_0/d = 0.002$. These conditions were selected to provide a maximum opportunity for a large angle-of-attack divergence so that a significant induced roll moment would be present. Furthermore, these asymmetries are sufficient to produce a first roll resonance lock-in. Such an instability would result in catastrophic failure.

Two-Fin Roll Control

The fin aerodynamic coefficients computed previously were incorporated into the trajectory simulation. The resulting performance parameters, shown in Fig. 8, illustrate the importance of the induced fin nonlinearities. The simulation with linear roll moment coefficients due to fin cant alone shows that the roll

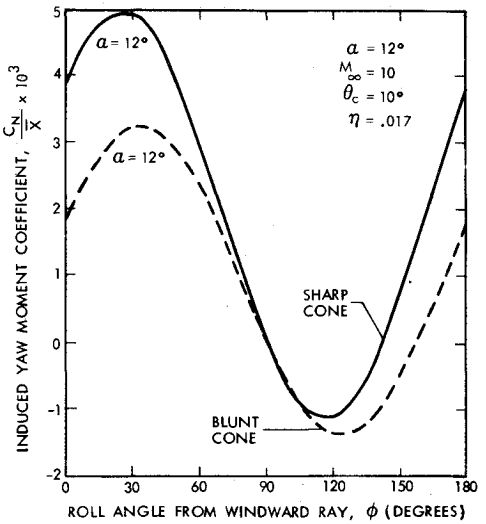

Fig. 7 Induced yawing moment coefficient for sharp and blunt cones vs roll orientation angle.

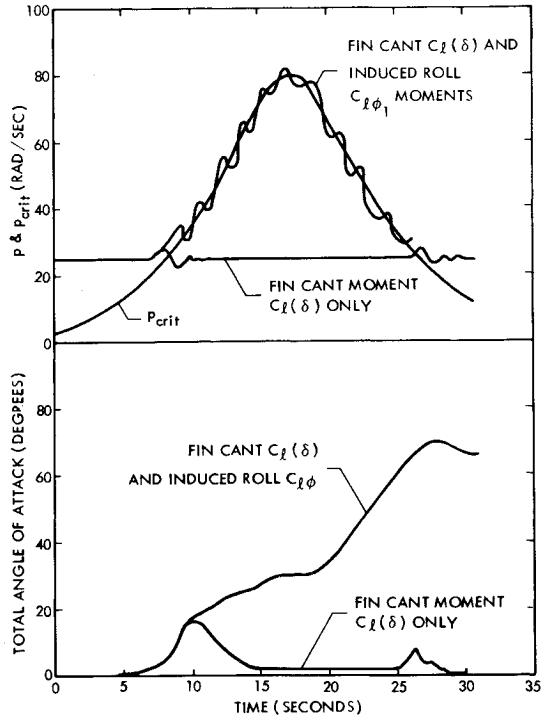

Fig. 8 Flight performance parameters for two-fin system with and without induced roll moment.

lock-in instability is controlled, and the angle-of-attack divergence remains within acceptable limits. However, with the nonlinear induced roll moment, the vehicle exhibits sustained resonance, and the angle of attack diverges to unacceptable values. Increasing the fin area would increase both the fin cant and the induced moments by the same factor, thus providing no net increase in effectiveness of the fin control system. The total fin cant cannot be increased greatly without incurring unacceptable fin loads. Clearly, the solution lies in reducing the induced roll moment. This reduction may be accomplished by including an additional pair of fins, diametrically opposed and in a plane normal to the first pair.

Four-Fin System

The four-fin system reduces the induced roll moment to acceptable values so that roll control may be obtained.[4] The roll orientation terms in Eq. (2) are nearly independent of fin deflection; thus, the second set of fins need not be canted to minimize the roll orientation dependence. For an uncanted pair, the first term in Eq. (2) vanishes, and $C_{l\phi_1}$ and $C_{l\phi_2}$ are evaluated for $\delta = 0$ and δ_c. The combined roll coefficient for both sets of fins is then expressed as

$$C_{l_{\text{total}}} = C_{l_{\delta_c}}(\alpha)\delta_c + \bar{C}_{l\phi_1}(\alpha, \delta_c)\sin 2\phi + \bar{C}_{l\phi_2}(\alpha, \delta_c)\cos 2\phi \quad (9)$$

where the overbar indicates the difference of induced roll terms, which vanish for $\delta_c = 0$.

A comparison of the induced roll moments for the two- and four-fin (with two at zero cant) systems are represented in Figs. 9 and 10 for the sharp and blunt cones, respectively. In either case, $\bar{C}_{l\phi_2}$ is quite small and is not presented. A significant reduction in roll-dependent coefficients is obtained for both configurations with a four-fin system, although the reduction is greater for the blunt cone. For the case of zero fin cant on the movable pair, the induced terms are reduced to zero. The results of the trajectory simulation for the four-fin system closely agree with those presented in Fig. 8 for the case of linear roll moment coefficient due to fin cant only, $C_l(\delta)$.

Flight Test Results

To verify the aerodynamic and flight dynamic analysis methods and to demonstrate the capability of the spin fin roll-control concept, the roll-control system was flight tested on the Sandia Re-entry Vehicle Resonance Test Vehicle (RVRTV).[6] The RVRTV program consists of a series of flights in which vehicles with various types of built-in asymmetries are flown to investigate flight dynamic behavior during both persistent and transient roll resonance. A two-stage Nike-Hercules rocket is used to boost the flight vehicle into a low-altitude, supersonic Mach number trajectory.

The conical flight vehicle external geometry is identical to that of the dynamic stability correlation models used by the Supersonic Tunnel Association and the AGARD[17] (that is, a cone half-angle of 10° and a nose-to-base radius ratio of 0.0167) and identical to that used in the sharp cone computations presented previously. The flight vehicle had mass and inertia asymmetries (these included a principal axis inclination relative to the vehicle aerodynamic centerline of 0.25° and an out-of-plane, center-of-mass offset of 0.100 in.) intentionally built in so that without roll rate control, a severe and persistent roll resonance instability would occur.

Uncontrolled Trajectory

A flight test without roll control[6] preceded the fin roll-control flight to demonstrate the persistent roll resonance (roll lock-in) behavior of the vehicle. Based on this information and the roll-control vehicle physical properties, the spin rate and total angle-of-attack histories for the uncontrolled vehicle were simulated

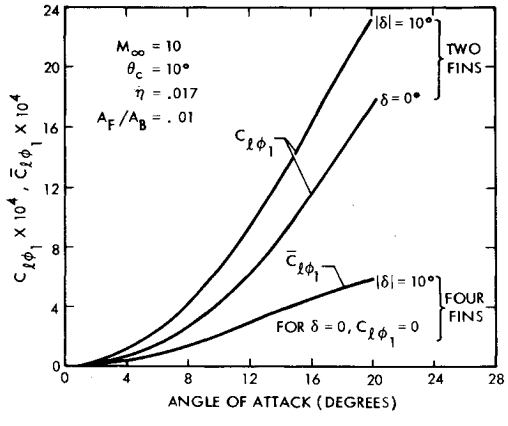

Fig. 9 Sharp cone induced roll moment coefficient for two-fin system $C_{l\phi_1}$ and for four-fin system $\bar{C}_{l\phi_1} = C_{l\phi_1}(\alpha, \delta) - C_{l\phi_1}(\alpha, 0)$.

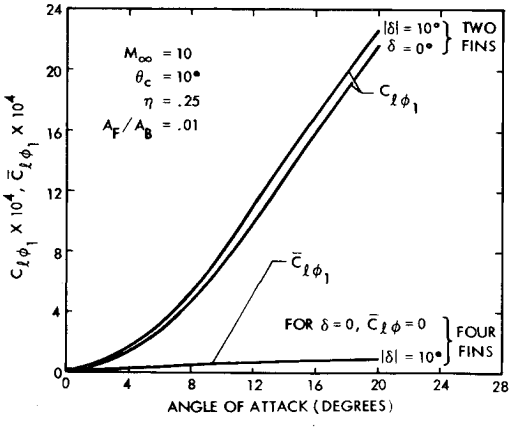

Fig. 10 Blunt cone induced roll moment coefficient for two-fin system $C_{l\phi_1}$ and for four-fin system $\bar{C}_{l\phi_1} = C_{l\phi_1}(\alpha, \delta) - C_{l\phi_1}(\alpha, 0)$.

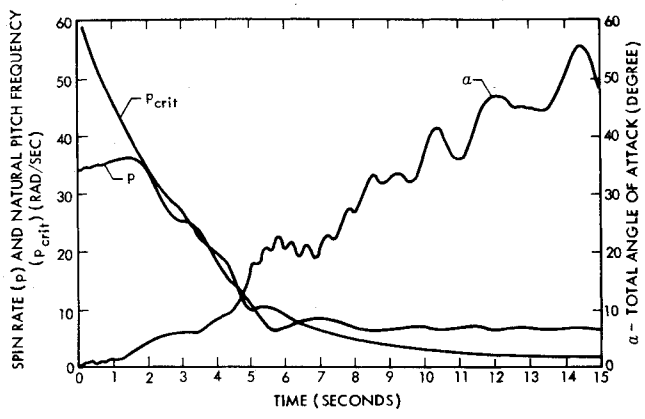

Fig. 11 Angle of attack, spin rate, and natural pitch frequency for uncontrolled trajectory.

(Fig. 11). The spin rate locks in to the vehicle natural pitch frequency (p_{crit}), thus exhibiting sustained roll resonance. The total angle of attack characteristically amplifies during this time and reaches values in excess of 60°, thus providing a meaningful and stringent test of the fin roll-control system capability. In addition, angles of attack sufficient to produce large fin nonlinearities are incurred.

Controlled Trajectory[4]

The flight parameters for the roll-control flight are shown in Fig. 12. The flight vehicle was launched at a spin rate below the control system design value, resulting in an initial spin-up into resonance. A spin-down phase from $T \cong 1.0$ to 3.2 sec indicates that the vehicle was in resonance. Note that the angle of attack (Fig. 12) exhibited a divergence during this time. Due to the action of the fin roll-control system, the vehicle recovers from the resonance instability at $T = 3.5$ sec, causing the angle of attack to converge. The results of the trajectory simulation, which incorporates the vehicle and control system properties, the initial conditions, and the theoretical and flight-derived aerodynamic

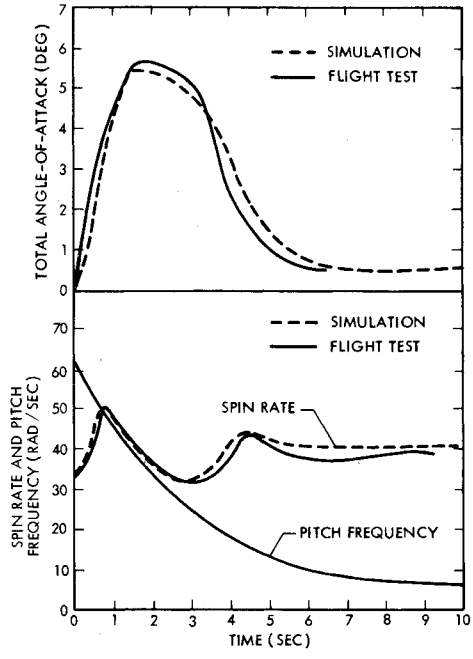

Fig. 12 Fin roll control vehicle flight test data and comparison with simulation.

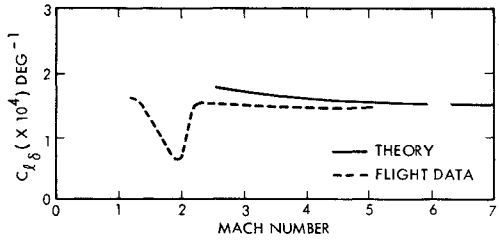

Fig. 13 Calculated and flight-derived fin cant roll moment coefficient C_{l_δ}.

characteristics are also shown with the flight data. An excellent agreement is obtained. The vehicle and fin aerodynamic characteristics were determined from a detailed analysis of the flight data.[4] These results indicate that the static stability was increased by about 20%, while the total drag coefficient was 30% higher than the flight data obtained on the same configuration without fins.

In Fig. 13, the flight-derived roll moment coefficient due to fin cant is shown to compare quite favorably with the calculated values down to a Mach number of about 2.5. Below Mach 2.5, the theory suggests an increase in fin effectiveness while the flight data indicate a relatively constant coefficient to Mach 2 and a sharp decrease below Mach 2.

Conclusions

The conclusions that follow from the results given in this paper are:

1) A computational method was developed which approximates the surface cross-flow on blunt cones and accurately predicts the nonlinear aerodynamic characteristics of finned reentry configurations.

2) The nonlinear induced roll coefficients are large enough to dominate the fin roll-control coefficient for small angles of attack. A four-fin system with two fixed fins and two variable cant fins reduces the induced roll moment to acceptable levels.

3) The analytical and simulation techniques accurately represented the actual flight performance of a four-fin system. Flight-derived fin coefficients are in excellent agreement with calculated values. The capability of the four-fin concept and the accuracy of the aerodynamic and flight dynamic analysis methods presented have been verified.

References

[1] Vaughn, H. R., "Spin-Up and Roll Reversal of Reentry Vehicles," SC-RR-68-219, May 1968, Sandia Labs., Albuquerque, N. Mex.

[2] Vaughn, H. R., "Boundary Conditions for Persistent Roll Resonance on Re-Entry Vehicles," *AIAA Journal*, Vol. 6, No. 6, June 1968, pp. 1030–1035.

[3] Hodapp, A. E., Jr. and Clark, E. L., Jr., "Effects of Products of Inertia on Re-Entry Vehicle Roll Behavior," *Journal of Spacecraft and Rockets*, Vol. 8, No. 2, Feb. 1971, pp. 155–161.

[4] Kryvoruka, J. K., "Flight Test Evaluation of a Reentry Vehicle Spin Fin Roll Control System," SCL-DR-720077, Nov. 1972, Sandia Labs., Livermore, Calif.

[5] Platus, D. H., "Dynamic Instability of Finned Missiles Caused by Unbalanced Fin Forces," *AIAA Journal*, Vol. 9, No. 3, March 1971, pp. 378–381.

[6] Hodapp, A. E., Jr. and Beckmann, R. C., "Flight Test Evaluation of a Fluidically Actuated Monopropellant Hydrazine Roll Control System," AIAA Paper 72-975, Palo Alto, Calif., 1972.

[7] Nicolaides, J. D., "Two Nonlinear Problems in the Flight Dynamics of Modern Ballistic Missiles," IAS Paper 59-17, New York, 1959.

[8] Chrusciel, G. T. and Hull, L. D., "Theoretical Method for Calculating Aerodynamic Characteristics of Spherically Blunted Cones," AIAA Paper 68-674, Los Angeles, Calif., 1968.

[9] Blick, E. F. and Francis, J. E., "Spherically Blunted Cone Pressure Distributions," *AIAA Journal*, Vol. 4, No. 3, March 1966, pp. 547–549.

[10] Eaton, R. R., "Numerical and Experimental Surface Pressure Distributions and Shock Shapes On 15-Degree Sphere Cones at Angles of Attack," SC-DR-69-0259, 1969, Sandia Labs., Albuquerque, N. Mex.
[11] Ashurst, W. T., "HANDY," SCL-DR-70-25, March 1970, Sandia Labs., Livermore, Calif.
[12] Babenko, K. I. et al., "Three-Dimensional Flow of Ideal Gas Past Smooth Bodies," TT-F-380, April 1966, NASA.
[13] Kryvoruka, J. K. and Ashurst, W. T., "Re-Entry Vehicle Finned Roll Rate Control: Aerodynamic and Flight Dynamic Analysis," AIAA Paper 73-183, Washington, D.C., 1973.
[14] Rakich, J. V. and Cleary, J. W., "Theoretical and Experimental Study of Supersonic Steady Flow around Inclined Bodies of Revolution," *AIAA Journal*, Vol. 8, No. 3, March 1970, pp. 511–518.
[15] George, O. L., Jr., "An Experimental Investigation of the Flow Field Around an Inclined Sharp Cone in Hypersonic Flow," SC-RR-69-577, Sept. 1969, Sandia Labs., Albuquerque, N. Mex.
[16] Kryvoruka, J. K., "A Formulation of the Equations of Motion for Flight Vehicles with Semi-Passive Roll Control Systems," SCL-RR-720007, April 1972, Sandia Labs., Livermore, Calif.
[17] Fail, R. and Garner, H. C., "Calibration Models for Dynamic Stability Tests," Rept. 563, 1968, Advisory Group for Aerodynamic Research and Development, Neuilly-sur-Seine, France.

MARCH 1974 J. SPACECRAFT VOL. 11, NO. 3

A Wind-Tunnel Study of Spinning Conical Disk Decelerators at Mach 4

ANTONI K. JAKUBOWSKI *
Virginia Polytechnic Institute and State University, Blacksburg, Va.

An experimental investigation was made of the aerodynamic torque and drag characteristics of several configurations of rotating conical disk models placed in a supersonic Mach 4 stream. A basic shape of 73° half angle was used and solid surface configurations as well as "porous" ones were tested. Experiments seem to indicate that at a given supersonic Mach number, the torque coefficient of a highly porous configuration can be approximately expressed as a function of a single variable parameter (Reynolds number related to the peripheral velocity) and two constants which depend on geometry of the disk. For a selected geometric configuration, torque coefficient is inversely proportional to the porosity of the surface. For solid surface disks, torque increases rapidly when grooves (or other "deformations") are present which are oriented in the radial direction. Circumferential grooves or slots produce only a relatively small torque increase. A suggestion is made about an aerodynamically "optimal" network of a spinning filamentary decelerator. Drag coefficient of rotating disks varies consistently with the degree of porosity. Within the range of spin rates tested, C_D remained constant, independent of rotation.

Nomenclature

A = reference area (maximum cross-sectional area of disk) πR^2
A_o = open surface area of disk
A_t = total surface of leading side of disk
C_D = drag force coefficient, $D/q_\infty A$
C_M = aerodynamic drag torque coefficient, $M_d/(\rho_\infty/2)\omega^2 R^5$
D = drag force
M = freestream Mach number
M_d = aerodynamic torque of conical disk (for porous configuration) or friction torque on the leading side of disk (for solid surface configuration)
q_∞ = freestream dynamic pressure
r = radius
R = maximum radius of disk
Re = Reynolds number
s = spin rate parameter, $\omega R/U$
U = freestream velocity
v = circumferential velocity in boundary layer
z = distance perpendicular to surface
λ = geometric porosity
μ = viscosity
ν = kinematic viscosity
ρ = density
ρ_∞ = freestream density
τ = shearing stress
ϕ = half-angle of conical disk
ω = angular velocity

Received June 8, 1973; revision received October 19, 1973. This work was supported by the VPI & SU Research Division Grant. The author wishes to thank J. Lukasiewicz for his advice and interest in this study and J. Van Overeem and W. A. Shirley for their assistance in the experimentation.
Index categories: Entry Deceleration Systems and Flight Mechanics (e.g. Parachutes); Supersonic and Hypersonic Flow.
* Assistant Professor, Aerospace Engineering. Member AIAA.

Introduction

A SPINNING flexible disk has been proposed[1,2] as a potential entry decelerator which offers many operational advantages such as large drag area combined with low decelerator weight fraction, effective radiation cooling, improved communication throughout the descent, and a potential for maneuvering. Such a decelerator can be formed, for instance, by a rapidly spinning filamentary disk mounted at its center to a hub on the nose of the capsule and maintained in an erected position by the centrifugal forces. The energy for the initial spin-up can be provided by small rocket motors mounted on the rim of the disk. For missions requiring maneuvering, the periphery of the disk may be equipped with a number of aerodynamic vanes to counteract the aerodynamic friction torque of the disk.

Aerodynamic analysis of a spinning disk decelerator requires